

Cluster Percolation in the Two-Dimensional Ising Spin Glass

L. Münster* and M. Weigel

Institut für Physik, Technische Universität Chemnitz, 09107 Chemnitz, Germany

(Dated: December 27, 2022)

Suitable cluster definitions have allowed researchers to describe many ordering transitions in spin systems as geometric phenomena related to percolation. For spin glasses and some other systems with quenched disorder, however, such a connection is missing to date. Using Monte Carlo simulations, we study the percolation properties of several classes of clusters occurring in the Edwards-Anderson Ising spin-glass model in two dimensions. The Fortuin-Kasteleyn–Coniglio-Klein clusters originally defined for the ferromagnetic problem do percolate at a temperature that remains non-zero in the thermodynamic limit. On the Nishimori line, this location is accurately predicted by an argument due to Yamaguchi [1, 2]. More relevant for the spin-glass transition are clusters defined on the basis of the overlap of several replicas. We show that various such cluster types have percolation thresholds that shift to lower temperature by increasing the system size, in agreement with the zero-temperature spin-glass transition in two dimensions. The overlap is linked to the difference in density of the two largest clusters, thus supporting a picture where the spin-glass transition corresponds to an emergent density difference of the two largest clusters inside the percolating phase.

PACS numbers: 75.40.Mg, 02.60.Pn, 68.35.Rh

I. INTRODUCTION

Cluster representations and droplet models provide a framework to study critical phenomena from the geometrical perspective of percolation [3–5]. For the Ising ferromagnet the most prominent schemes are the Fortuin-Kasteleyn cluster representation [4, 6] as well as a microscopic definition of Fisher droplets [7] introduced by Coniglio and Klein [8, 9]. Both approaches eventually lead to the same cluster definition. These Fortuin-Kasteleyn–Coniglio-Klein (FKCK) clusters represent thermal fluctuations, the percolation temperature is equivalent to the critical temperature of the ferromagnetic phase transition and the critical exponents of this thermal transition are linked to those of the percolation transition [4, 9]. Furthermore, such clusters unveil interesting properties of the problem that are not accessible from the free energy of the Ising model [9]. Apart from these physical aspects, FKCK clusters are also the basis of powerful Monte Carlo cluster methods such as the Swendsen-Wang algorithm [10, 11] which dramatically reduces the critical slowing down observed in the vicinity of the transition that affects simulations with purely local update schemes.

In contrast to the case of the Ising ferromagnet, FKCK clusters in models with frustration such as spin glasses [12–15] do not have an obvious physical meaning [16], which is a consequence of the fact that by construction the growth of such clusters signals the increase of ferro/antiferromagnetic correlations and not ordering of the spin-glass nature. Other types of clusters may hence show more interesting behavior when studying such frustrated systems. The order parameter of the spin-glass

transition, the overlap, is defined with respect to two replicas. Therefore, it seems natural to consider cluster definitions which include multiple replicas. Here we investigate in detail three different types of two-replica clusters, each of which can be linked to the overlap. The simplest of them just groups together spin sites with identical value of the overlap. These clusters are the basis of the Houdayer cluster algorithm [17], which is why we denote them as Houdayer clusters. A more elaborate cluster definition can be extracted from a graphical representation initially proposed by Chayes, Machta and Redner for spin systems in external fields [18, 19] that also allows for a cluster representation of the Ising spin-glass model [20]. Due to an additional connection to another cluster algorithm for (dilute) spin glasses proposed by Jörg [21], we refer to these clusters as Chayes-Machta-Redner-Jörg (CMRJ) clusters. And thirdly, we study a cluster definition which was introduced by Newman and Stein as a generalization of the FKCK clusters to more than one replica [22]. These structures we denote as two-replica FKCK (2R-FKCK) clusters.

The CMRJ and 2R-FKCK clusters were already studied numerically for the three-dimensional Ising spin glass and analytically for the Sherrington-Kirkpatrick (SK) model which corresponds to the mean-field description of spin glasses [20]. In three dimensions, the CMRJ and 2R-FKCK clusters are found to percolate at a temperature above the spin-glass transition, while the spin-glass transition itself can be related to an emergent density difference of the two largest clusters [20]. In contrast, in two dimensions the spin-glass transition occurs at zero-temperature, so it will be interesting to see how the percolation behavior changes in this scenario. A better understanding of cluster structures in spin glasses might help to develop more efficient Monte Carlo cluster algorithms for these systems, hence bringing equilibrium

* lambert.muenster@physik.tu-chemnitz.de

studies of larger systems into the reach of numerical simulation methods [23] which are urgently needed due to the strong finite-size effects in spin-glass physics [24].

The rest of this article is organized as follows. In Sec. II the Ising spin-glass model is introduced and the simulation methods are described. In Sec. III we report on our study of the FKCK clusters in a spin glass with a interaction distribution symmetric around zero as well as on the Nishimori line. In particular, we compare our results to a conjecture regarding the exact location of the transition point [2]. In the following Sections we present our numerical results for the two-replica cluster definitions, namely for the CMRJ clusters in Sec. IV, the 2R-FKCK clusters in Sec. V, as well as the Houdayer clusters in Sec. VI. Finally, Sec. VII contains our conclusions.

II. MODEL AND NUMERICAL METHODS

We consider the two-dimensional Ising spin glass with Gaussian interactions. The Hamiltonian is given by

$$H_J(\mathbf{S}) = - \sum_{\langle \mathbf{x}, \mathbf{y} \rangle} J_{\mathbf{x}\mathbf{y}} s_{\mathbf{x}} s_{\mathbf{y}}. \quad (1)$$

The system contains N spins which sit on the sites of a square lattice of linear size L , such that $N = L^2$. The sum runs over all nearest-neighbor spin pairs as indicated by the notation $\langle \mathbf{x}, \mathbf{y} \rangle$ for lattice vectors \mathbf{x} and \mathbf{y} . In this study only fully periodic boundary conditions are used. \mathbf{S} denotes a configuration of Ising spins $s_{\mathbf{x}} = \pm 1$, i.e., $\mathbf{S} \in \{\pm 1\}^N$. The quenched interactions between the spins are represented by bonds $J_{\mathbf{x}\mathbf{y}}$ that are drawn from a Gaussian distribution with standard deviation σ_J and mean J_0 ; we write $\mathbf{J} = \{J_{\mathbf{x}\mathbf{y}}\}$ for the coupling realization. As a consequence bonds can be ferromagnetic (positive) or antiferromagnetic (negative). A bond is said to be satisfied if $J_{\mathbf{x}\mathbf{y}} s_{\mathbf{x}} s_{\mathbf{y}} > 0$ and it is broken if $J_{\mathbf{x}\mathbf{y}} s_{\mathbf{x}} s_{\mathbf{y}} < 0$. If there does not exist a spin configuration such that all bonds are satisfied simultaneously, the system is referred to as frustrated. The two-dimensional model undergoes a zero-temperature spin-glass transition [25–30]. The order parameter of the spin-glass transition, the Parisi overlap parameter [12], is defined with respect to two replicas $\mathbf{S}^{(1)}$ and $\mathbf{S}^{(2)}$,

$$q(\mathbf{S}^{(1)}, \mathbf{S}^{(2)}) = \frac{1}{N} \sum_{\mathbf{x}} s_{\mathbf{x}}^{(1)} s_{\mathbf{x}}^{(2)} = \frac{1}{N} \sum_{\mathbf{x}} q_{\mathbf{x}}, \quad (2)$$

where $q_{\mathbf{x}} = s_{\mathbf{x}}^{(1)} s_{\mathbf{x}}^{(2)}$. Replicas are spin configurations $\mathbf{S}^{(1)}, \mathbf{S}^{(2)}, \dots$ of a system at the same inverse temperature β which evolve independently in time but share the same realization of bonds. In the high-temperature phase the absolute value of the overlap approaches zero and its distribution in the thermodynamic limit is a delta peak at the origin. At low temperature spins have the tendency to point in a direction such that the bonds are satisfied and they hence freeze into suitable metastable states. As

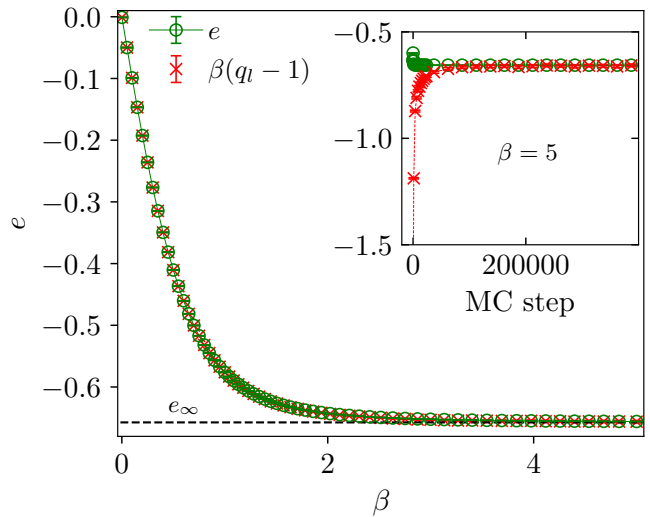


FIG. 1. Internal energy per bond, e , of the 2D Ising spin glass of Eq. (1) as a function of inverse temperature β at system size $L = 128$ averaged over 500 realizations of the bonds. The data for the shifted and scaled link overlap $\beta(q_l - 1)$ demonstrates that the equilibration condition of Eq. (5) is fulfilled within error bars at all temperatures. The inset shows the convergence to equilibrium at the lowest temperature ($\beta = 5$) for an average over 50 disorder realizations at the lowest temperature. To ensure that the system is in equilibrium we start sampling after 4×10^5 MC steps. The dotted line illustrates the value of the ground state energy $e_{\infty} = -0.6573938(4)$ according to Ref. [31].

a consequence, below the spin-glass temperature the distribution of the absolute value of the overlap has a mean which is larger than zero.

To study the model at a range of temperatures we employ Monte Carlo simulations techniques. To obtain reliable numerical results it is important to ensure that the system is in equilibrium. As a reliable indicator to signal equilibration we use a relation that was established in [32] for short-range spin glasses. It is based on the fact that mathematically speaking Eq. (1) defines a Gaussian variable with a covariance that is proportional to the link overlap, q_l , i.e.

$$[H_J(\mathbf{S}^{(1)}) H_J(\mathbf{S}^{(2)})]_J = N_b q_l(\mathbf{S}^{(1)}, \mathbf{S}^{(2)}) \quad (3)$$

for $J_0 = 0$ and $\sigma_J = 1$ [33]. N_b is the number of bonds and $[\dots]_J$ denotes the disorder average with respect to the bond distribution. The link overlap is given by

$$q_l(\mathbf{S}^{(1)}, \mathbf{S}^{(2)}) = \frac{1}{N_b} \sum_{\langle \mathbf{x}, \mathbf{y} \rangle} s_{\mathbf{x}}^{(1)} s_{\mathbf{y}}^{(1)} s_{\mathbf{x}}^{(2)} s_{\mathbf{y}}^{(2)}. \quad (4)$$

This connection between covariance of the Hamiltonian and the link overlap has important implications. One consequence is that the energy per bond can be expressed in terms of the link overlap [32, 33]

$$e = \beta(q_l - 1), \quad (5)$$

where $e = [\langle H_J(\mathbf{S}) \rangle_S]_J / N_b$. Keep in mind that here it is necessary to consider the disorder average with respect to the bond distribution $[\dots]_J$ as well as the configurational average with respect to the Boltzmann distribution $\langle \dots \rangle_S$. When the system is initialized randomly, the energy decreases during the equilibration process and the value of the link overlap increases as is shown in the inset of Fig. 1, and in equilibrium Eq. (5) is satisfied. Note that as demonstrated by Contucci *et al.* [33–36], it is possible to derive further important properties from relation (3), which underlines the significance of the link overlap in short-range spin glasses [37].

In order to determine the overlap, we simulate in parallel two replicas at each temperature. A Monte Carlo step of our procedure consists of four individual parts. A single spin-flip Metropolis sweep, an FKCK cluster move with a Wolff update [38], and alternately a Houdayer [17] or a Jörg cluster move [21] at each even or odd Monte Carlo time step, respectively. For the latter we use a Swendsen-Wang type update rule [38] which ensures that also smaller clusters are flipped in the percolating phase. At the end of each Monte Carlo step we perform an exchange Monte Carlo move [39] of replicas at neighboring temperatures. The details of the different cluster moves will be described in the Sections below. While the replica-exchange component is mandatory to achieve equilibration, the specific mix of different cluster and single-spin flip moves chosen here is empirically found to perform well, but we do not claim that this is the optimal protocol for the problem. Figure 1 demonstrates that the energy monotonously decreases with a declining slope when lowering the temperature. At the lowest considered temperature the energy $e(\beta = 5) = -0.65591(13)$ at system size $L = 128$ is already close to that of the ground state of the infinite system, $e_\infty = -0.6573938(4)$ [31].

To the extent that self-averaging is present in the model, it is possible to reduce the number of bond realizations to compute the disorder averages by increasing the system size. At the FKCK percolation transition the Wolff cluster updates are extremely effective and we equilibrate 2000 bond realizations for the largest considered system size, $L = 512$, and up to 12 500 bond realizations for the smallest system size, $L = 64$. In the lower temperature region down to $\beta = 5$ the equilibration process needs much more time. In this case we use between 500 bond realizations for the largest system size, $L = 128$, and 7000 bond realizations for the smallest size $L = 16$.

III. THE FKCK PERCOLATION TRANSITION

In this Section we introduce essential observables which characterize percolation using the example of the FKCK percolation transition in the two-dimensional Ising spin glass with Gaussian interactions. Furthermore we numerically test the prediction of Yamaguchi [1, 2] who conjectured an exact critical temperature for the percolation transition on the Nishimori line.

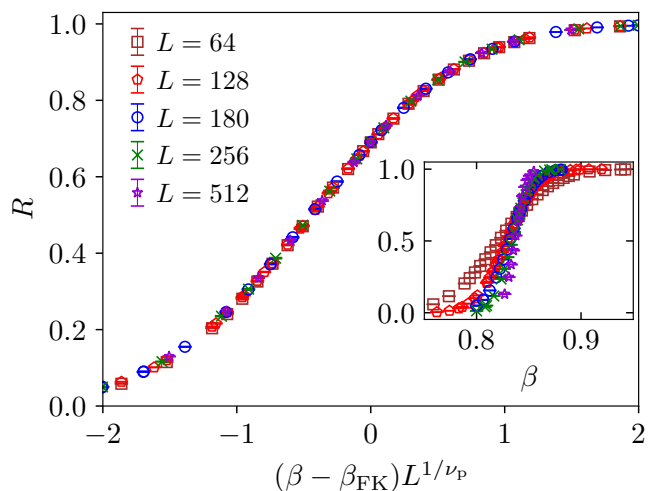


FIG. 2. Scaling of the wrapping probability in case of the FKCK percolation transition of the standard 2D Ising spin glass with $J_0 = 0$, $\sigma_J = 1$. The data collapse is achieved according to Eq.(8) with $\beta_{\text{FK}} = 0.84079(17)$ and $1/\nu_p = 0.749(4)$. The inset shows the unscaled data for the different system sizes.

In standard random-bond percolation all bonds are occupied independently with the same probability $p_{\mathbf{x}\mathbf{y}} = p$. In the correlated FKCK percolation problem, on the other hand, bonds are occupied with probability

$$p_{\mathbf{x}\mathbf{y}} = \begin{cases} 1 - e^{-2\beta|J_{\mathbf{x}\mathbf{y}}|} & \text{if } J_{\mathbf{x}\mathbf{y}}s_{\mathbf{x}}s_{\mathbf{y}} > 0 \\ 0 & \text{else} \end{cases}. \quad (6)$$

Thus, the occupation probability depends on the spin configuration. Occupied bonds connect spin sites which group together in clusters. The smallest possible cluster contains a single spin site. These clusters are denoted in the following as FKCK clusters. Depending on the literature they are also called CK droplets [8] or FK clusters [6]. Starting from this it is possible to define cluster updates. Flipping each cluster with probability $\frac{1}{2}$ corresponds to the Swendsen-Wang update rule [11]. Constructing only one cluster from a randomly chosen seed site by adding bonds with the probability given in Eq. (6) and always flipping it gives the Wolff update rule [38, 40]. By flipping a cluster we mean that each spin inside the cluster is reversed in sign. Both, the Swendsen-Wang as well as the Wolff cluster update define ergodic Monte Carlo algorithms that satisfy the detailed balance condition with respect to the Boltzmann distribution [41].

In case of the Ising ferromagnet the probability of two spins pointing in the same direction at two different lattice sites, \mathbf{x} , \mathbf{y} , is equal to the probability that the two lattice sites are connected by a path of occupied bonds,

$$\langle s_{\mathbf{x}}s_{\mathbf{y}} \rangle_S = \text{Prob}(\mathbf{x} \text{ and } \mathbf{y} \text{ are connected by occupied bonds}). \quad (7)$$

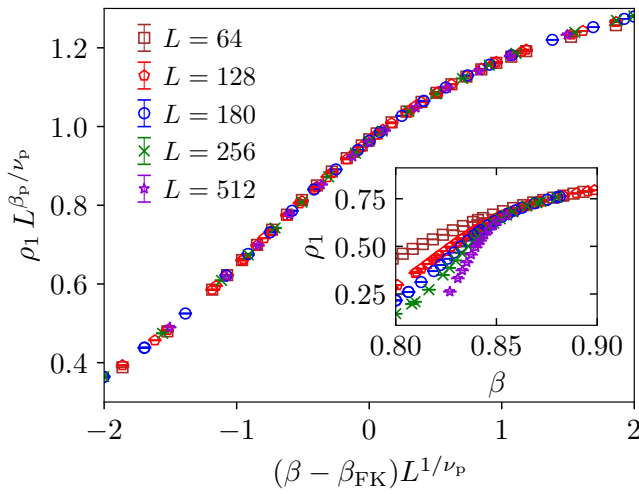


FIG. 3. The density of the largest cluster as a function of inverse temperature for the FKCK percolation transition of the standard 2D Ising spin glass with $J_0 = 0$, $\sigma_J = 1$. The main plot shows a data collapse according to Eq. (9) with $\beta_{FK} = 0.8411(5)$, $1/\nu_p = 0.754(18)$ and $\beta_p/\nu_p = 0.101(6)$. The inset shows the unscaled data for the different system sizes.

In other words, the two-spin correlation function is equal to the pair-connectness function of the FKCK percolation problem [4, 9]. Thus, the percolation transition must coincide with the ferromagnetic phase transition. Due to frustration this relation is absent in spin glasses [42, 43] and the percolation transition has no obvious physical interpretation. (Note that these clusters are areas of satisfied bonds and not of parallel spins, so they do not represent ferromagnetic order.) It occurs at a higher temperature than the spin-glass transition, in the vicinity of the dynamic damage spreading transition [16, 44], and it shows the characteristics of a random (uncorrelated) percolation transition [3]. Just above the temperature $1/\beta_{FK}$, a single giant cluster begins to form, the so-called incipient infinite cluster. Here, β_{FK} denotes the inverse temperature at which percolation takes place in an infinitely large system. In the numerically studied finite systems with fully periodic boundaries the condition of percolation is satisfied if there exists a path of connected occupied bonds that wraps around the boundary in the horizontal direction, in the vertical direction, or in both directions. The probability R for such wrapping to occur thus provides information about the location of the percolation transition. Finite-size scaling (FSS) implied that it behaves as [3]

$$R(\beta, L) = f_R \left((\beta - \beta_{FK}) L^{1/\nu_p} \right) \quad (8)$$

close to criticality, where f_R is a scaling function. The order parameter of the percolation transition can be defined as the density of the largest cluster ρ_1 (often denoted as ρ_∞) which is given by the fraction of sites in

J_0	σ_J	$1/\nu_p$	β_p/ν_p	γ_p/ν_p	β_{FK}
0	1	0.749(4)	0.101(6)	1.7920(8)	0.84079(17)
$\text{erf}^{-1}(1/2)\sqrt{2}$	1	0.750(7)	0.102(5)	1.7904(7)	0.67447(8)
bond percolation		3/4	5/48	43/24	$p_{th} = 1/2$
(numerical)		0.75	$0.1041\bar{6}$	$1.791\bar{6}$	$p_{th} = 0.5$

TABLE I. Overview of the critical exponents and inverse percolation temperatures in case of the FKCK percolation transition. The table shows the results for the standard Ising spin glass $J_0 = 0$, $\sigma_J = 1$ as well as for $J_0 = \text{erf}^{-1}(1/2)\sqrt{2}$, $\sigma_J = 1$. In the bottom line we show the exact values for random bond percolation in two dimensions. p_{th} denotes the percolation threshold. The data collapse of the FSS analysis is performed with the tool given in [46].

the cluster that contains the most spin sites. Inside the percolating phase the largest cluster corresponds to the infinite cluster for $L \rightarrow \infty$. The density of the largest clusters satisfies the scaling form [3]

$$\rho_1(\beta, L) = L^{-\beta_p/\nu_p} f_{\rho_1} \left((\beta - \beta_{FK}) L^{1/\nu_p} \right). \quad (9)$$

In the Ising ferromagnet this observable corresponds to the absolute value of the magnetization per site [9]. Another quantity of interest is the mean cluster size [9],

$$\chi_p = \sum_{s=1} s^2 n(s). \quad (10)$$

In the paramagnetic phase of the Ising ferromagnet this quantity is equal to the magnetic susceptibility [9]. The sum runs over all sizes (masses) of clusters, s , except the infinite cluster; $n(s)$ is the cluster number per site which equals the average number of clusters of size s divided by N . At the critical point the mean cluster size diverges as $\chi_p(\beta_{FK}) \sim L^{\gamma_p/\nu_p}$, described by the exponent γ_p/ν_p [45].

In case of the standard Ising spin glass with Gaussian interactions, $J_0 = 0$ and $\sigma_J = 1$, we perform Monte Carlo simulations and measure the observables R , ρ_1 and χ_p of the FKCK clusters. The data collapse of R and ρ_1 are illustrated in Figs. 2 and 3, respectively. The results for the critical exponents are $1/\nu_p = 0.749(4)$ and $\beta_p/\nu_p = 0.101(6)$. The estimated critical temperature of the percolation transition, extracted from the data of R , is $\beta_{FK} = 0.84079(17)$. To receive γ_p/ν_p we fit a power law to the data of the mean cluster size for different system sizes at inverse temperature $\beta = 0.84085$ which corresponds to an inverse temperature of the Monte Carlo simulation between the estimates of β_{FK} from R and ρ_1 . This leads to the critical exponent $\gamma_p/\nu_p = 1.7920(8)$. Note that in order to compute χ_p we do *not* exclude the percolating cluster as this was found to reduce finite-size effects, a phenomenon which was also observed in previous work [47, 48]. The critical parameters extracted from the data via FSS are collected in Table I. The data collapse of the FSS analysis are performed with the tool given in [46]. The statistical error is computed by generating 150 bootstrap samples of

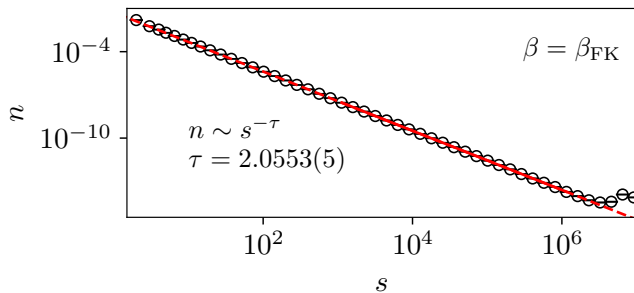


FIG. 4. The cluster number n as a function of cluster size s at the percolation threshold on the Nishimori line, $\beta_{\text{FK}} = \text{erf}^{-1}(1/2)\sqrt{2} = 0.67448975\dots$. The system size is $L = 4096$. On the Nishimori line the energy is $e(\beta_{\text{FK}}) = -J_0$ [51]. The simulation gives $e(\beta_{\text{FK}}) = -0.674490(11)$, a sign that the system is in equilibrium. The disorder average is computed with respect to 125 bond samples.

the data and individually performing a data collapse for each sample. The systematic error is estimated by varying the range of the considered data which is used to perform the collapse from $(\beta - \beta_{\text{FK}}) L^{1/\nu_p} \in [-0.35, 0.35]$ to $(\beta - \beta_{\text{FK}}) L^{1/\nu_p} \in [-1, 1]$. Both, the statistical and the systematic contribution are summed to give the final estimate of the error.

The critical exponents are consistent with the universality class of random percolation. The correlations which arise since only satisfied bonds can be occupied and the influence of the varying bond strength do not change the universality of the percolation transition. This result is expected to be stable also when $J_0 \neq 0$ [44, 49, 50].

For the special case of the Nishimori line, the FKCK percolation transition has been investigated by Yamaguchi [1, 2]. The Nishimori line is a certain set in parameter space of β and J_0/σ_J at which it is possible to analytically compute the internal energy and other quantities via a gauge transformation [52]. Yamaguchi was able to derive a condition for the critical bond occupation probability of the FKCK clusters, and he conjectured that it is identical to the percolation threshold of random-bond percolation. This conjecture provides a prediction for the critical inverse temperature,

$$\beta_{\text{FK}} = J_0/\sigma_J = \text{erf}^{-1}(1/2)\sqrt{2} = 0.67448975\dots \quad (11)$$

The conjecture is tested by performing simulations on the Nishimori line with $J_0 = \text{erf}^{-1}(1/2)\sqrt{2}$ and $\sigma_J = 1$. We carry out the same FSS scaling analysis for the data of R , ρ_1 and χ_p at the critical temperature, $\beta = \text{erf}^{-1}(1/2)\sqrt{2}$, as previously discussed for the standard Ising spin glass. All the results are compiled in the third line of Table I. Our estimate of the critical temperature $\beta_{\text{FK}} = 0.67447(8)$ is consistent with the value in Eq. (11).

At the critical point the cluster number $n(s)$ as well as the cluster radius $r(s)$ are expected to follow power laws $n \sim s^{-\tau}$ and $r \sim s^{1/d_f}$, respectively. The radius of

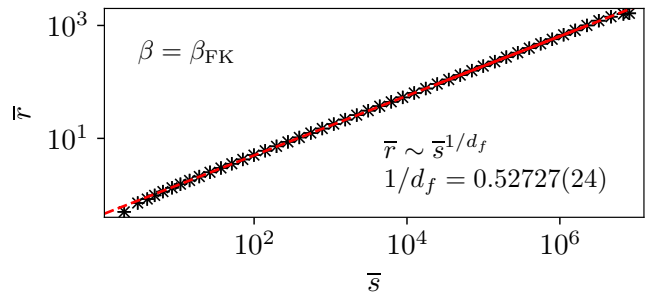


FIG. 5. The cluster radius as a function of cluster size on the Nishimori line with $\beta_{\text{FK}} = \text{erf}^{-1}(1/2)\sqrt{2}$. For the data analysis we used a logarithmic binning of the cluster sizes. The average size of the clusters within a bin is denoted as \bar{s} and the corresponding average radius is given by \bar{r} . The system size is $L = 4096$. The disorder average is computed with respect to 125 bond samples.

a cluster is defined as [3]

$$r(s) = \sqrt{\frac{\sum_{k=1}^s |\mathbf{r}_k - \mathbf{r}_c|^2}{s}}. \quad (12)$$

The sum corresponds to the average Euclidean distance of all sites \mathbf{r}_k of the cluster from its center of mass \mathbf{r}_c . For non-percolating clusters the center of mass can simply be derived from the average distance to the origin of the coordinate system. As the origin we chose the root of the cluster. For percolating clusters we used the algorithm proposed in Ref. [53]. Figures 4 and 5 show the cluster number and the cluster radius at $\beta_{\text{FK}} = \text{erf}^{-1}(1/2)\sqrt{2}$, respectively. The values for $\tau = 2.0552(4)$ and for the fractal surface dimension $d_f = 1.8966(9)$ are consistent with random percolation because the exact values are $\tau = 187/91 = 2.054945$ and $d_f = 91/48 = 1.8958\bar{3}$, respectively. The data further supports the conjecture from Yamaguchi of a random-bond percolation transition at $\beta_{\text{FK}} = \text{erf}^{-1}(1/2)\sqrt{2}$. Altogether the results are in agreement with the idea that the FKCK transition in Ising spin glasses belongs to the random bond-percolation universality class.

IV. CMRJ CLUSTERS

The order parameter of the spin-glass transition, the overlap, is defined with respect to two replicas. It is hence natural to construct clusters related to the spin-glass transition by considering the overlap of several replicas. Such clusters might additionally turn out to be useful for designing effective Monte Carlo cluster algorithms. Proposals along these lines were already put forward rather early on by Swendsen and Wang in Ref. [39]. In the following, we investigate the properties of a particular type of multiple-replica clusters. The occupation probability

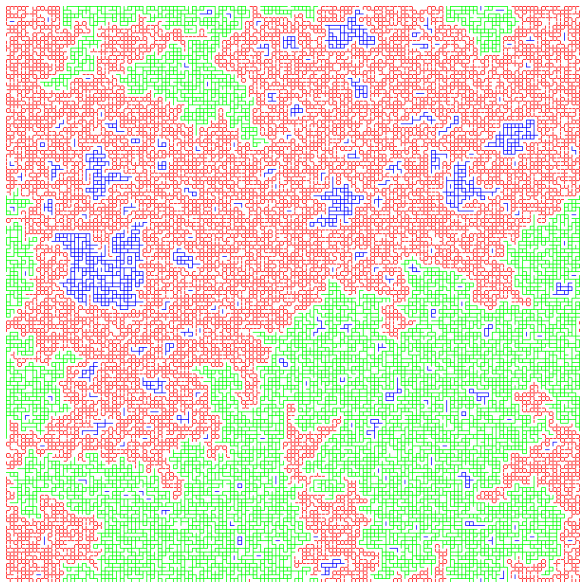


FIG. 6. Typical example of CMRJ clusters at $\beta = 3$ in thermal equilibrium, extracted from a simulation of a 152×152 sample of the Gaussian 2D Ising spin glass using two replicas. The red bonds belong to the largest cluster and the green bonds to the second largest cluster. Both clusters have an opposite sign of the overlap. The blue bonds are part of smaller clusters. Unoccupied bonds are white.

of the clusters for I replicas is given by

$$p_{\mathbf{x}\mathbf{y}} = \begin{cases} 1 - \exp(-2\beta J_{\mathbf{x}\mathbf{y}} \tilde{s}_{\mathbf{x}} \tilde{s}_{\mathbf{y}}) & \text{if } J_{\mathbf{x}\mathbf{y}} \tilde{s}_{\mathbf{x}} \tilde{s}_{\mathbf{y}} > 0 \\ 0 & \text{else} \end{cases},$$

$$\text{with } \tilde{s}_{\mathbf{x}} \tilde{s}_{\mathbf{y}} = \sum_{i=1}^I s_{\mathbf{x}}^{(i)} s_{\mathbf{y}}^{(i)}, \quad (13)$$

where i is the replica index and $\tilde{s}_{\mathbf{x}} = (s_{\mathbf{x}}^{(1)}, \dots, s_{\mathbf{x}}^{(I)})$ denotes an I -component spin. This is a generalization of the cluster definition proposed by Chayes, Machta and Redner [18–20] as well as by Jörg [21] to more than two replicas. The condition $J_{\mathbf{x}\mathbf{y}} \tilde{s}_{\mathbf{x}} \tilde{s}_{\mathbf{y}} > 0$ enforces the constraint that only those bonds are occupied which are satisfied simultaneously in the majority of the replicas [54]. Clusters are defined as spin sites which are connected by a path of occupied bonds. A cluster move can then be realized by flipping all I -component spins $\tilde{s}_{\mathbf{x}}$ within the same cluster, i.e., $\tilde{s}_{\mathbf{x}} \rightarrow -\tilde{s}_{\mathbf{x}}$ for all \mathbf{x} inside the cluster. As for the FKCK clusters, this can be done in a single-cluster or multi-cluster fashion as in the Wolff [38] and Swendsen-Wang [10] algorithms, respectively. Such a procedure aims to generate equilibrium states according to the I -replica Boltzmann distribution

$$\mathcal{P}(\mathbf{S}^{(1)}, \dots, \mathbf{S}^{(I)} | \mathbf{J}) = Z_{\mathbf{J}}^{-I} \exp\left(-\beta H_{\mathbf{J}}^{(I)}\right)$$

$$\text{with } H_{\mathbf{J}}^{(I)}(\mathbf{S}^{(1)}, \dots, \mathbf{S}^{(I)}) = - \sum_{\langle \mathbf{x}, \mathbf{y} \rangle} J_{\mathbf{x}\mathbf{y}} \tilde{s}_{\mathbf{x}} \tilde{s}_{\mathbf{y}} \quad (14)$$

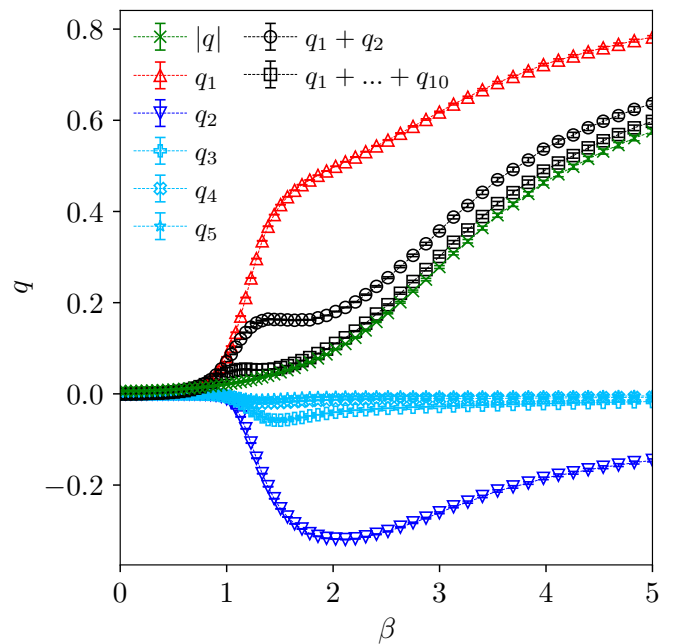


FIG. 7. Overlap of the CMRJ clusters at system size $L = 128$ averaged over 500 bond realizations. $|q|$ denotes the average value of the overlap per site which is the order parameter of the spin-glass transition. q_k is the overlap density of the k -th largest cluster, corresponding to the density of the cluster multiplied by the sign of its overlap. The relative spin orientation of the replicas is chosen such that the sign of the overlap of the largest cluster is always positive. We see that the largest and the second largest cluster are anticorrelated with respect to the sign of the overlap. The sum of the overlap densities of the largest clusters approaches $|q|$. Already $q_1 + q_2$ is almost parallel to $|q|$ for $\beta > 2$.

where $Z_{\mathbf{J}}$ is the partition function of a single replica for a given realization of the bonds \mathbf{J} .

To check for the convergence of the corresponding Markov chain, we need to investigate (detailed) balance and ergodicity [41]. That detailed balance holds with respect to the distribution (14) can be derived from the cluster surface energy with respect to the I -replica Hamiltonian, $H_{\mathbf{J}}^{(I)}$, that is the sum of the energies of the individual replicas. We provide this derivation in Appendix A. Since during cluster moves the overlap of any two replicas, $q_{\mathbf{x}} = s_{\mathbf{x}}^{(i)} s_{\mathbf{x}}^{(j)}$, $i, j = 1, 2, \dots, I$, $i \neq j$, is conserved, such cluster flips are not ergodic, however. In case of $I = 2$ the described cluster algorithm corresponds to the method proposed by Jörg [21] which has been successfully applied to simulate diluted spin glasses [55]. Since an equivalent cluster definition does also emerge from the graphical representation of Chayes, Machta and Redner [18–20] connected occupied components of this kind are denoted here as CMRJ clusters [56]. In the following we focus on the case of $I = 2$ which is, of course, of special significance for spin glasses. This is due to the fact that all spins within the same CMRJ cluster have identi-

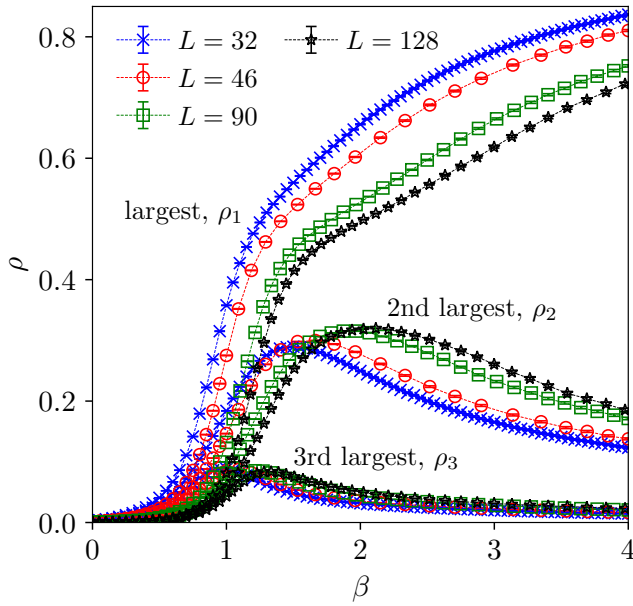


FIG. 8. Density $\rho = s/N$ of the three largest CMRJ clusters for different system sizes L . The curves shift to lower temperature when the system size is increased. The height of the peak of the second largest cluster increases whereas the peak of the third largest cluster decreases.

cal sign of the overlap. As a consequence, it is plausible to ask the question how these cluster are linked to the overlap especially in connection with the spin-glass transition.

Fig. 6 illustrates an instance of CMRJ clusters of a sample of the 2D Gaussian spin glass at $\beta = 3$ in thermal equilibrium. There are mainly two large clusters. As is illustrated in Fig. 7, this is a typical constellation at low temperatures. This plot shows the overlap density of the five largest clusters as well as the average overlap, $|q| = [\langle |q(\mathbf{S}^{(1)}, \mathbf{S}^{(2)})| \rangle_S]_J$. The overlap density of a cluster is defined as the density of a cluster multiplied by the sign of its overlap. The relative orientation of the spins of the replicas is chosen such that the largest cluster has positive overlap. The overlap density of the second largest cluster, q_2 , is anticorrelated in sign with respect to the largest cluster. The sum of the overlap densities $q_1 + q_2$ is almost parallel to $|q|$ for $\beta > 2$. This observation supports the idea that the difference in density of the two largest clusters is proportional to $|q|$ at low temperature [20]. The overlap increases on lowering the temperature and for $\beta \rightarrow \infty$ it approaches one as then the system reaches the ground state [28] and all spins are contained in a single CMRJ cluster.

Fig. 8 shows the density of the three largest CMRJ clusters at different system sizes. Again it is observed that the two largest clusters contain most of the spin sites at low temperature. The curves shift to lower temperature by increasing the system size. The height of the peak of the second largest cluster increases whereas that

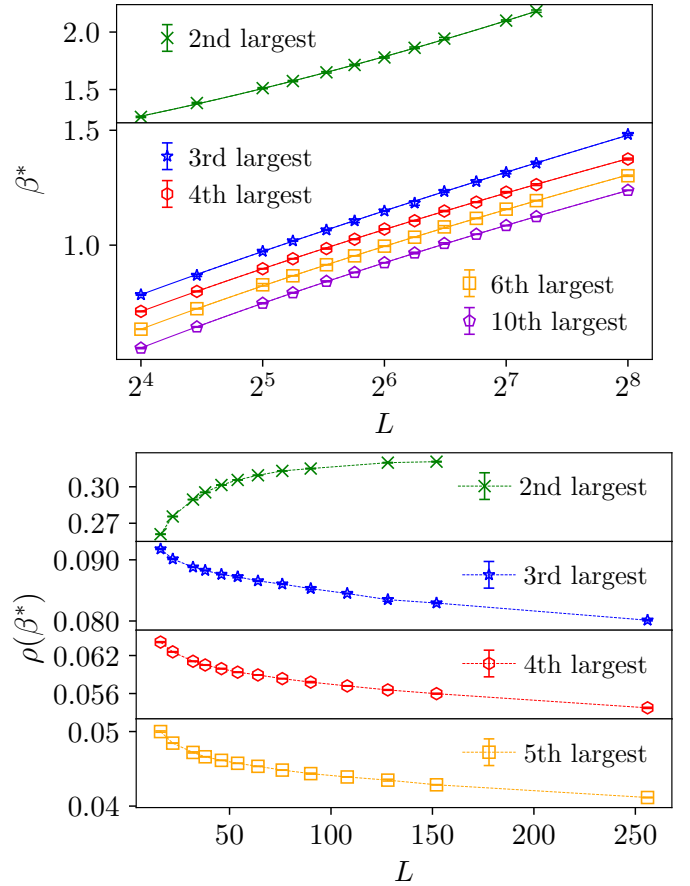


FIG. 9. Scaling of the peaks of the second largest and smaller CMRJ clusters. The upper panel shows the location of the peak, β^* , of the k -th largest clusters as a function of system size. The lines are fits of the functional form $\beta^*(L) = c_1 \ln(L)^{c_2} + c_3$, where c_1, c_2 , and c_3 are fit parameters. The lower panel shows the density of the corresponding clusters at their peak location. The density of the second largest cluster increases in contrast to that of the smaller clusters. The dotted lines are guides to the eye.

of the of smaller clusters decrease. This is of some significance since if the contribution of the third largest and smaller clusters becomes negligible for $L \rightarrow \infty$ the overlap approaches the difference in the density of the two largest clusters. A scenario of this type was proposed in Ref. [20] which also provides a rigorous proof for the SK model.

To better understand this aspect, properties of the peaks of the densities of the largest clusters are investigated in more detail. The location and height of the peak are extracted from the data by fitting parabolas in the vicinity of the peaks. Error bars are obtained via parabola fits of 250 bootstrap samples as described in Ref. [57]. The results are depicted in Fig. 9. The locations β^* of the peaks shift to smaller temperatures as the system size is increased. The density of the second largest cluster increases with system size, whereas that of smaller clusters decreases. Therefore, the influence of

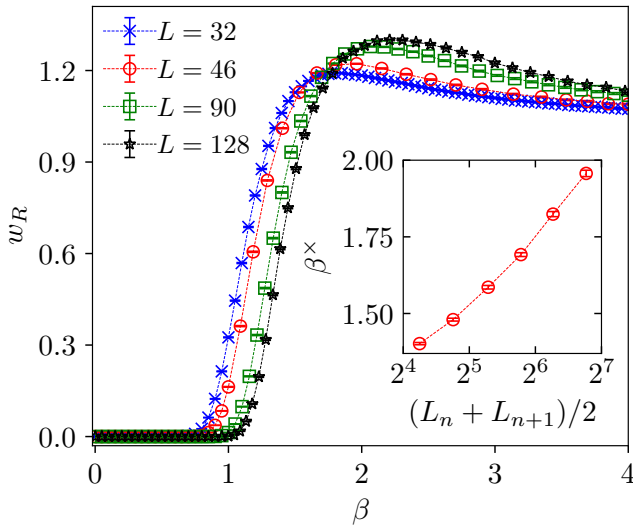


FIG. 10. Number of wrapping CMRJ clusters w_R as a function of inverse temperature for different system sizes. The inset shows the crossing points β^\times of two neighboring system sizes with $L = (16, 22, 32, 46, 64, 90, 128)$. The lines are guides to the eyes only.

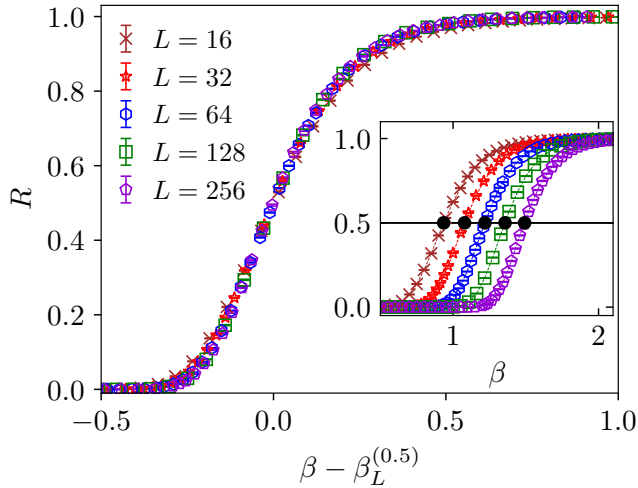


FIG. 11. Wrapping probability of the CMRJ clusters for different system sizes. The inset shows the unscaled data. The solid black points correspond to the inverse temperatures at which the wrapping probability is one half, $R(\beta_L^{(0.5)}) = 0.5$. The main plot shows a collapse of the data onto a single curve obtained by a shift of the data along the x -axis by the corresponding value of $\beta_L^{(0.5)}$.

the smaller clusters diminishes by increasing L , which is consistent to the idea that the overlap becomes equal to the difference in density of the two largest clusters in the thermodynamic limit [20].

The percolation transition of the CMRJ clusters does not fit in the framework of a random percolation transition. The latter features a single incipient infinite cluster which forms at the percolation transition, while the

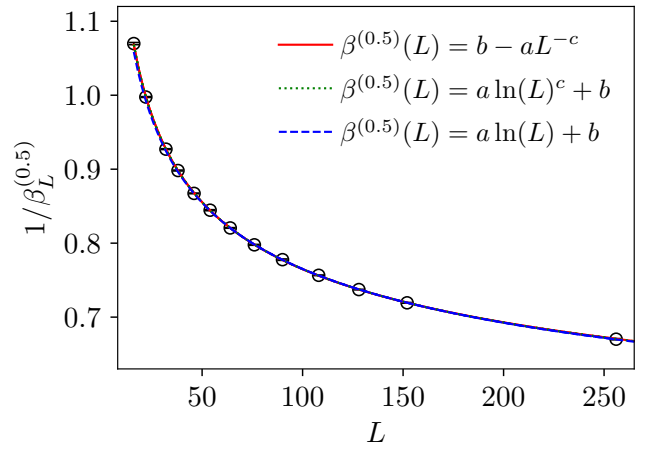


FIG. 12. The plot demonstrates how the percolation transition shifts to lower temperature $T = 1/\beta$ as the system size is increased. The temperature at which the wrapping probability is one half, $1/\beta_L^{(0.5)}$, is plotted as a function of L . The lines are fits of different type. The logarithmic law $\beta^{(0.5)}(L) = a \ln(L) + b$ is only consistent with the data for large system sizes.

former shows two giant clusters that develop a density difference at the spin-glass transition. Therefore, it is interesting to investigate whether both clusters can wrap simultaneously around the boundaries, similar to what is observed in three dimensions [20]. The data in Fig. 10 demonstrate that this is the case for finite systems, since on average there is more than one wrapping cluster in the temperature region where the system starts to percolate. For $\beta \rightarrow \infty$, w_R is expected to approach one since in the ground state there is only one giant CMRJ cluster left that contains all spins. The inset of Fig. 10 shows the crossing points β^\times of w_R of two adjacent system sizes from the list $L = (16, 22, 32, 46, 64, 90, 128)$ which are expected to behave like pseudo-critical temperatures of the problem. The crossing points shift to larger β in agreement with the behavior of the peak locations shown in Fig. 9.

An alternative definition of pseudo-critical temperatures results from a consideration of the wrapping probability R . The inset of Fig. 11 depicts R for different system sizes. It is observed that for increasing L the curves shift to larger β along the x -axis. We define pseudo-critical points as the inverse temperatures at which the wrapping probability is one half, i.e., $R(\beta_L^{(0.5)}) = 0.5$. These values are determined by spline interpolation of the data and their error bars are generated with bootstrapping. The main plot of Fig. 11 shows a data collapse of R which is obtained by shifting the data along the x -axis by the values of $\beta_L^{(0.5)}$. The estimated values of $\beta_L^{(0.5)}$ are shown individually in Fig. 12. They can be well described by the functional form $\beta^{(0.5)}(L) = a \ln(L)^c + b$ with $a = 0.260(13)$, $b = 0.289(20)$ and $c = 0.894(20)$ where the minimal considered system size is $L_{\min} = 16$.

and the quality of the fit is $Q = 0.87$. A simpler logarithmic law with $c = 1$, namely $\beta^{(0.5)} = a \ln(L) + b$, only yields good results for larger system sizes $L_{\min} = 64$ with $a = 0.1978(10)$, $b = 0.396(5)$ and $Q = 0.60$. These fits do suggest a zero temperature percolation transition in the thermodynamic limit, since $1/\beta_L^{(0.5)} \rightarrow 0$ when $L \rightarrow \infty$. Note that a power law of the form $\beta^{(0.5)}(L) = b - aL^{-c}$ can also be fitted to the data, resulting in $a = 8.5(1.5)$, $b = 8.8(1.5)$, $c = 0.026(6)$ with $L_{\min} = 16$ and $Q = 0.81$. This would imply a finite-temperature transition [58] with a critical inverse temperature of $8.8(1.5)$. However, in view of the small value $c = 0.026(6)$ of the exponent, a fit of the form $a \ln(L)^c + b$ appears to be much more natural. Additionally, the pure power-law fit strongly depends on L_{\min} , such that already for $L_{\min} = 46$ the error bars exceed the values of the fit parameters. Finally, the positive curvature in the peak locations of the second largest cluster and in the crossing points of the number of wrapping clusters, see Figs. 9 and 10, rather support the idea of a zero-temperature transition. To sum up, our results are in good agreement with the scenario of a zero-temperature percolation transition.

The spin-glass transition occurs at a temperature below the percolation transition, and it is connected to the difference in density of the two largest clusters [20]. Therefore, both above discussed scenarios, a finite-temperature or a zero-temperature percolation transition, are consistent with the zero-temperature spin-glass transition in two dimensions. The pseudo-critical temperatures that describe the spin-glass transition shift towards zero temperature with a power-law behavior according to $T_{\text{SG}}(L) \sim L^{-1/\nu}$ [28, 29], where $1/\nu = 0.2793(3)$ [31]. This is much faster than the asymptotically logarithmic scaling of the pseudo-critical temperatures of the percolation transition as shown in Fig. 12.

V. TWO-REPLICA FKCK CLUSTERS

Another approach towards a multiple-replica cluster definition is to connect FKCK clusters of different replicas. A straightforward definition of such clusters is given by the occupation probability

$$p_{\mathbf{x}\mathbf{y}} = \begin{cases} (1 - e^{-2\beta|J_{\mathbf{x}\mathbf{y}}|})^I & \text{if } J_{\mathbf{x}\mathbf{y}}\tilde{s}_{\mathbf{x}}\tilde{s}_{\mathbf{y}} > 0 \text{ and } |\tilde{s}_{\mathbf{x}}\tilde{s}_{\mathbf{y}}| = I \\ 0 & \text{else} \end{cases}$$

$$\text{where } \tilde{s}_{\mathbf{x}}\tilde{s}_{\mathbf{y}} = \sum_{i=1}^I s_{\mathbf{x}}^{(i)} s_{\mathbf{y}}^{(i)}. \quad (15)$$

This means only those bonds can be occupied which are satisfied in all I replicas simultaneously. The occupation probability is equal to the event that in all I replicas the bond is occupied individually with the probability of the FKCK clusters, see Eq. (6). In the present paper, we focus on the scenario of $I = 2$ and connected components are denoted as 2R-FKCK clusters [59]. Spins within the same 2R-FKCK cluster have the same overlap. These

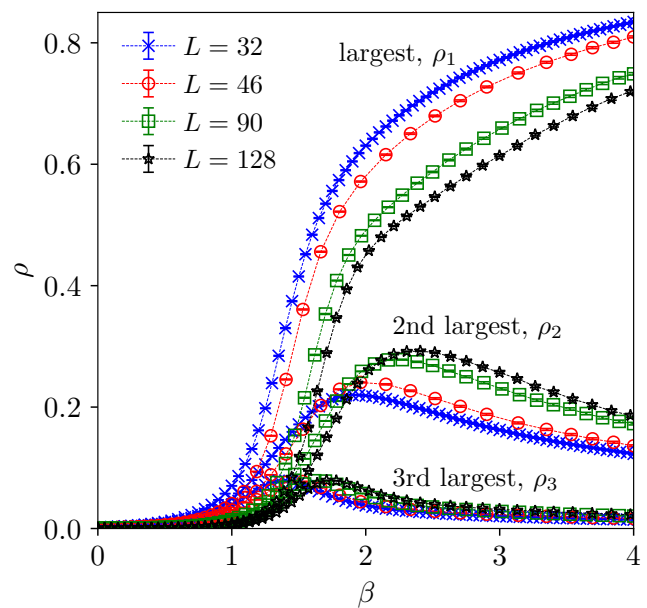


FIG. 13. Density of the three largest 2R-FKCK clusters at different system sizes. The curves shift to lower temperature when the system size is increased.

2R-FKCK clusters were initially proposed by Newman and Stein with the aim of providing tools to mathematically show broken spin-flip symmetry in short-range spin glasses at non-zero temperature [22].

Although there is rather strong numerical evidence for a finite-temperature spin glass phase for $d \geq 3$ [26, 27, 30, 60, 61] we do not have a rigorous proof. In the case of a ferromagnet it can be shown that the appearance of a unique largest percolating FKCK cluster corresponds to the onset of long-range order and broken symmetry [9]. In spin glasses, FKCK percolation is a necessary condition for broken symmetry and the occurrence of a unique largest 2R-FKCK cluster is a sufficient condition [62]. Furthermore, in the SK model the difference in density of the two largest 2R-FKCK clusters is equal to the overlap and thus directly connected to the spin-glass transition. Note that, in case of the SK model this is also true for the previously discussed CMRJ clusters. In the three-dimensional Ising spin glass a similar behavior is expected. Although there is some numerical evidence in favor of this scenario [62], it is not entirely clear if the difference in density of the two largest clusters is precisely equal to the overlap or the contributions of smaller clusters are also relevant. In two dimensions there is no finite-temperature spin glass transition, and it is hence of particular interest to see what happens in this case.

Figure 13 shows the density of the three largest 2R-FKCK clusters. In general, the percolation transition has rather similar properties to the CMRJ one. In the vicinity of the transition there are two dominating clusters which can wrap simultaneously around the boundaries.

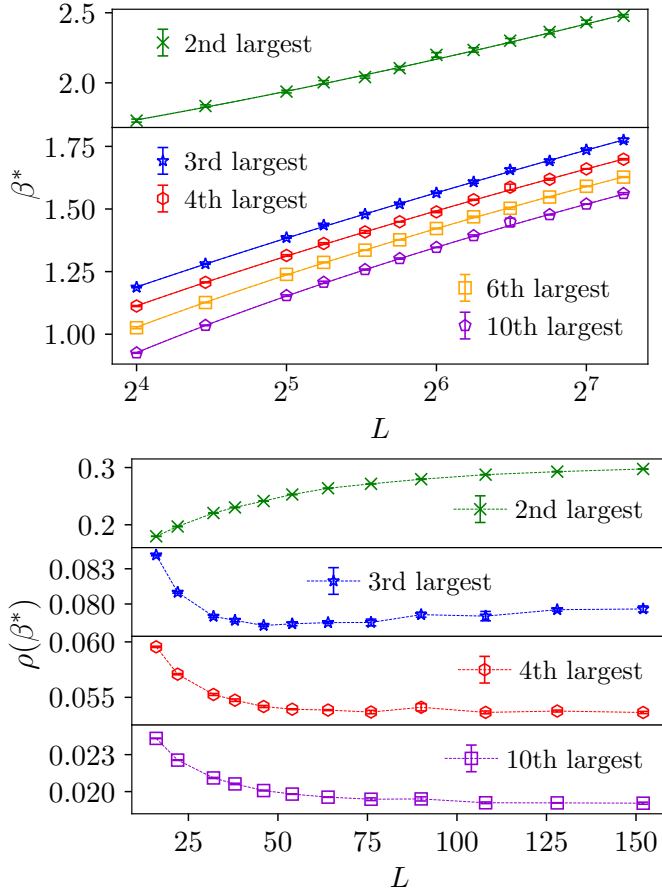


FIG. 14. Properties of the peaks of the second largest and smaller 2R-FKCK clusters. The upper panel shows the location of the peak β^* of the largest clusters as a function of system size. The lines are fits of the form $\beta^*(L) = c_1 \ln(L)^{c_2} + c_3$ to the data. The lower panel shows the density of the clusters at the peak locations. The density of the second largest cluster increases whereas the density of the smaller clusters show no clear trend for large system sizes.

These two largest clusters are anticorrelated with respect to the sign of the overlap and their difference in density is roughly proportional to the average overlap at low temperatures. In Fig. 14 we present the scaling of the peaks in the density of the second largest and smaller clusters. As is shown in the upper panel, the peak positions shift to lower temperatures as the system size is increased. The lower panel visualizes the peak densities of the largest clusters. It is visible that the height of the peak for the second largest cluster increases. The heights of the third largest and smaller clusters do not show a clear trend. Therefore, the evidence for an equality between the difference in density of the two largest clusters and the overlap is less convincing for the 2R-FKCK clusters than in case of the CMRJ clusters, cf. Fig. 9.

To further investigate the properties of 2R-FKCK clusters, we also considered the wrapping probabilities which are shown in Fig. 15. The data show a clear shift along

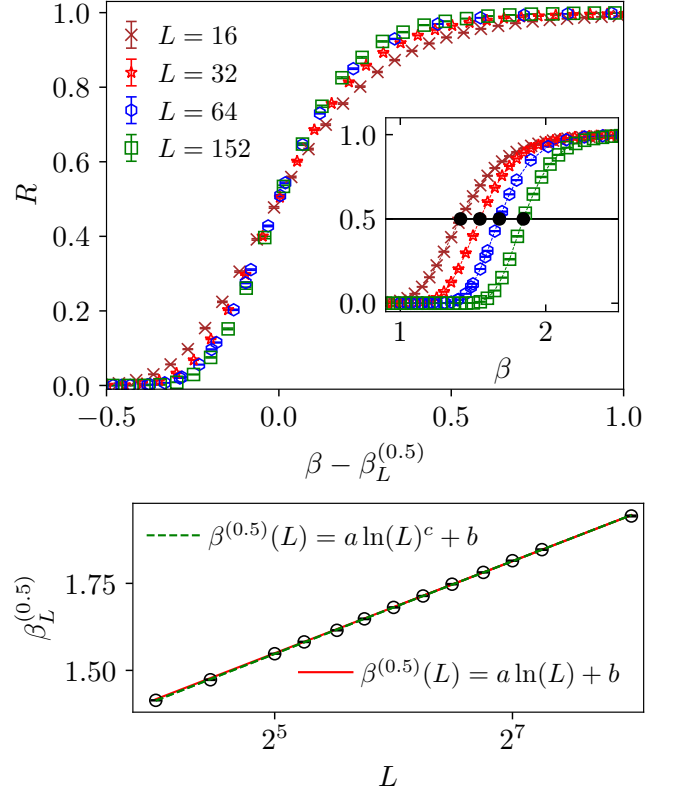


FIG. 15. Wrapping probability of the 2R-FKCK clusters for different system size. The upper panel shows the wrapping probability as a function of inverse temperature β for a number of the considered system sizes L . The inset contains the curves of the unscaled data. In the main plot there is a collapse of the data onto a single curve, which was obtained by a shift of the curves along the x -axis by the values of $\beta_L^{(0.5)}$. In the lower panel, these shifts are shown as a function of L ; they can be described by a logarithmic law of the type $a \ln(L)^c + b$ where c is close to one.

the x -axis to lower temperatures as the system size is increased. The shift is well described by a logarithmic law, i.e. $\beta^{(0.5)}(L) = a \ln(L)^c + b$ with $a = 0.206(14)$, $b = 0.859(22)$, $c = 0.972(28)$ and $L_{\min} = 16$. If the exponent is fixed to $c = 1$ and $L_{\min} = 64$ chosen the result is $a = 0.1908(15)$ and $b = 0.888(7)$. This is similar to the situation of the CMRJ clusters where the slope is $a = 0.1978(10)$. A power-law fit of the form $\beta^{(0.5)}(L) = b - aL^{-c}$ does not yield a satisfactory result.

The shift of the percolation transition towards zero temperature demonstrates that there is no sufficient condition for a broken spin-flip symmetry in two dimensions at finite temperatures. This observation is in agreement with previous numerical studies which show that there is no finite-temperature spin-glass phase in this case [25–27, 30, 60, 61]. Furthermore, it is consistent with the argument that is not possible to simultaneously have two infinitely large clusters with opposing order parameter in two dimensions in the thermodynamic limit, simply because there is not enough space [62, 63]. Note that the

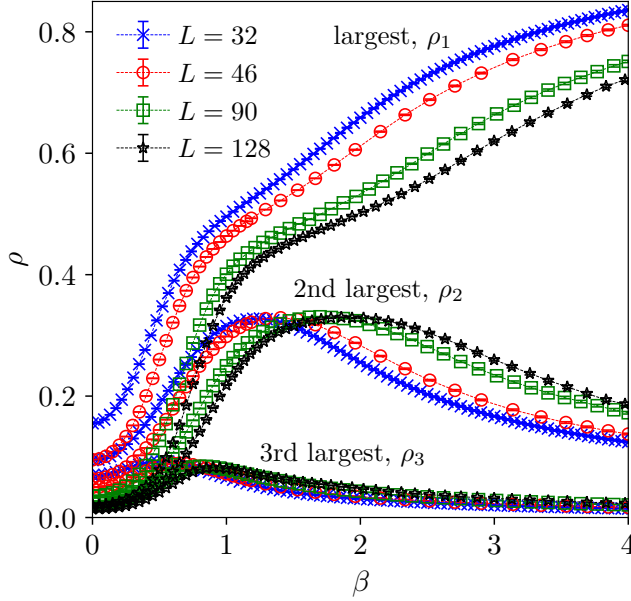


FIG. 16. Density of the three largest Houdayer clusters for different system sizes.

appearance of a single largest percolating CMRJ cluster would also imply broken symmetry [62].

VI. HOUDAYER CLUSTERS

Finally, we consider clusters of spin sites with the same overlap. These geometrical overlap-cluster are used in Houdayer's cluster algorithm which allows one to speed up the Monte Carlo simulation of spin glasses, at least in two dimensions [17, 64]. These clusters are closely analogous to geometrical clusters in case of the Ising ferromagnet [47]. The occupation probability is given by

$$p_{xy} = \begin{cases} 1 & \text{if } |\tilde{s}_x \tilde{s}_y| = 2 \\ 0 & \text{else} \end{cases} \quad (16)$$

and the number of replicas is two. Thus, clusters are simply defined as connected components of spin sites with identical overlap. These clusters have a vanishing surface energy within the energy of the $I = 2$ Boltzmann distribution, see Eq. (14), since $\tilde{s}_x \tilde{s}_y = 0$ at the cluster surface. Therefore, flipping the spins in these clusters in both replicas simultaneously, $\tilde{s}_x \rightarrow -\tilde{s}_x$, is in agreement with the detailed balance condition. Because the two-replica energy and the overlap are conserved quantities, such cluster moves are not ergodic. Note that any two adjacent clusters necessarily have an opposite sign of the overlap, and the sum over all bonds along the surface of the clusters is proportional to the link overlap (up to an additive constant) [37]. The previously discussed CMRJ and 2R-FKCK cluster are geometric subregions of the Houdayer clusters because each Houdayer cluster

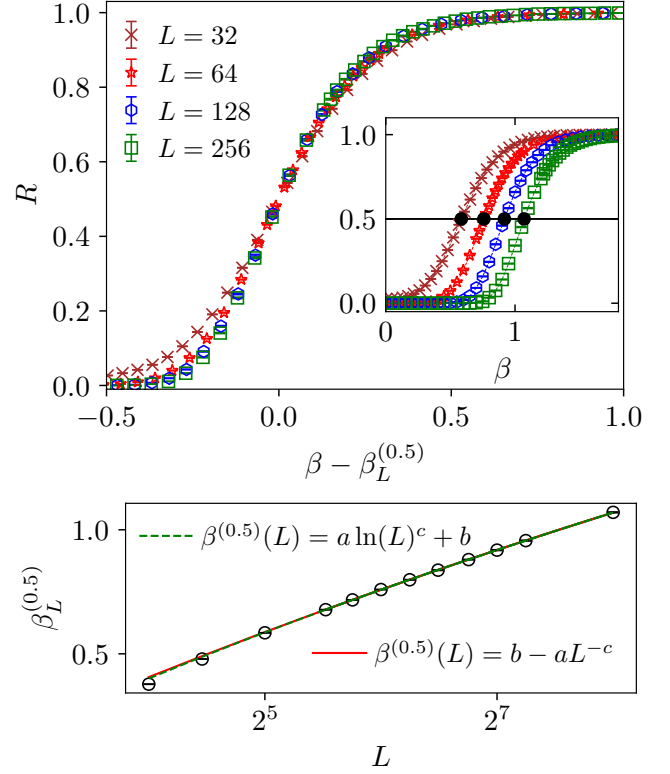


FIG. 17. Wrapping probability of Houdayer clusters in dependency of system size. The upper panel shows the wrapping probability for various system sizes. The inset contains the original data. In the main plot there is a collapse of the data onto a single curve, which was obtained by a shift of the curves along the x -axis by the values of $\beta_L^{(0.5)}$. The lower panel contains the data for the shifts $\beta_L^{(0.5)}$, together with a fit of the functional form $a \ln(L)^c + b$ with $L_{\min} = 46$.

includes all connected spin sites with identical overlap, irrespective of whether the underlying bonds are satisfied or not. Therefore, it might be expected that Houdayer clusters show similar properties. In fact, Fig. 16 demonstrates that, again, there are mainly two large clusters. In the vicinity of the percolation transition we again find that there is more than one wrapping cluster (not shown). Since the occupation probability does not depend on temperature, the wrapping probability can already be non-zero in the high-temperature regime. The percolation transition shifts to lower temperature as is shown in Fig. 17. The shift is consistent with a fit of the form $\beta^{(0.5)}(L) = a \ln(L)^c + b$ with $a = 0.73(12)$, $b = -0.93(15)$ and $c = 0.59(6)$ with $Q = 0.68$ and $L_{\min} = 46$. The data can also be fitted to a power law, $\beta^{(0.5)}(L) = b - aL^{-c}$ with $a = 3.85(29)$, $b = 3.4(4)$, $c = 0.090(12)$, $L_{\min} = 46$ and $Q = 0.56$. Again the exponent $c = 0.090(12)$ is so small that the fit does not contradict a logarithmic law.

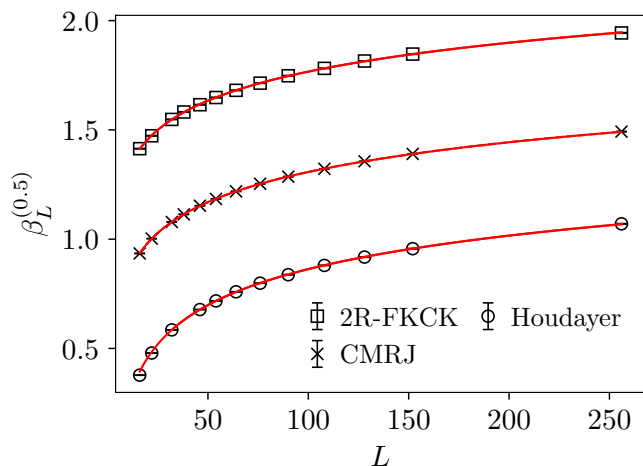


FIG. 18. Overview of the shift in the wrapping probabilities for the three cluster types, namely 2R-FKCK, CMRJ and Houdayer. The plot shows the value of the inverse temperature at which the wrapping probability is one half $R(\beta_L^{(0.5)}) = 0.5$. The lines are fits of type $\beta^{(0.5)}(L) = a \ln(L)^c + b$.

VII. DISCUSSION

We have studied percolation properties of the two-dimensional Ising spin glass with Gaussian interactions by performing Monte Carlo simulations. In the Ising ferromagnet Fortuin-Kasteleyn–Coniglio-Klein (FKCK) percolation is directly linked to the thermal phase transition. In spin glasses the FKCK percolation transition occurs at a higher temperature than the spin glass transition close to the heat-bath damage-spreading transition [65]. We find that the percolation threshold is $\beta_{\text{FK}} = 0.84085(8)$ in case of the standard spin glass where the mean of the Gaussian interaction distribution is zero, $J_0 = 0$, and the standard deviation is one, $\sigma_J = 1$. The transition belongs to the universality class of random percolation. On the Nishimori line [52], which is a certain line in the parameter space of J_0 and σ_J , Yamaguchi conjectured an exact inverse temperature of percolation [1, 2]. This conjecture agrees within error bars with the numerical data of our analysis. See also [65] for the case of a bimodal $\pm J$ interaction distribution.

The order parameter of the spin-glass transition, the overlap, is defined with respect to two replicas which suggests to study clusters which are defined with respect to two replicas. Thus, three different cluster types are considered, namely Chayes-Machta-Redner-Jörg (CMRJ), 2-replica-FKCK and Houdayer clusters where spins that belong to the same cluster have identical overlap. In all considered cases the pseudo-critical temperature of the percolation transition shifts to lower temperatures as the system size is increased. This is demonstrated in Fig. 18. The shift is well described by a functional form of $\beta^{(0.5)}(L) = a \ln(L)^c + b$ as the fits demonstrate. This behavior implies a zero temperature percolation transi-

tion in the thermodynamic limit. Furthermore, it is visible that the Houdayer clusters percolate at the highest temperature followed by the CMRJ clusters and the 2R-FKCK clusters at a given system size L . This relative order of clusters is a consequence of the fact that the CMRJ clusters as well as the 2R-FKCK clusters are geometric subregions of the Houdayer clusters since there only bonds can be occupied which are satisfied in both replicas. The occupation probability of the CMRJ clusters is higher than that of 2R-FKCK which explains why the CMRJ clusters percolate at a higher temperature than the 2R-FKCK clusters.

In all considered cluster definitions percolation is characterized by two large clusters which can simultaneously wrap around the boundaries close to the transition. These two largest clusters are anticorrelated with respect to the sign of the overlap. Furthermore, at low temperatures the mean overlap is proportional to the difference in density of the two largest clusters. In case of the CMRJ clusters it is visible that the density of the second largest cluster increases with system size whereas that of the smaller clusters decreases. In this scenario, the mean overlap equals the difference in density of the two largest clusters in the thermodynamic limit as proposed and shown for the SK model in Ref. [62]. Thus, if smaller clusters are irrelevant the dominance of the largest cluster over the second largest cluster is directly linked to the spin-glass transition. It is well known that pseudo-critical temperatures of the spin-glass transition shift to zero temperature in a power-law fashion with $\beta_{\text{SG}}(L) \sim L^{1/\nu}$ [28, 29], where $1/\nu = 0.2793(3)$ [31]. Since this power law decays much faster than the above discussed logarithmic law, the percolation transitions will always appear at a higher temperature as compared to the effective spin-glass transition at a given system size.

In case of the Ising ferromagnet FKCK clusters correspond to Fisher droplets and the pair-connectness function of the percolation problem is equal to the two-spin correlation function [9]. Thus, the percolation transition coincides with the thermal phase transition, which makes Monte Carlo cluster dynamics such as the Swendsen-Wang or Wolff algorithm very efficient close to criticality. This relation is absent in case of the considered two-replica cluster definitions and percolation takes place at a higher temperature than the spin-glass transition. At low temperatures there are mainly two large clusters which contain almost all spins. To identify clusters where the pair-connectedness function is linked directly to the overlap-correlation function seems to be an important goal for further studies. In other words, $\langle q_{\mathbf{x}} q_{\mathbf{y}} \rangle_s$ has to be proportional to the probability that the lattice sites \mathbf{x} and \mathbf{y} are connected by a path of occupied bonds for a given realization of interactions \mathbf{J} . If these clusters could be constructed in a computationally efficient way this would probably also lead to an effective cluster algorithm to study the spin-glass transition. In terms of cluster updates which reduce equilibration time and autocorrelation time it might also be useful to consider

more sophisticated computational methods. An interesting Ansatz would be to define multiple-replica clusters within the framework of the generalized cluster algorithm [66, 67]. Furthermore, it also appear promising to consider the use of machine learning techniques to identify clusters or to look at other non-local update schemes [68–71]. It hence remains an attractive but so far elusive goal to arrive at a full description of the spin-glass transition in terms of the percolation of clusters that directly propagate the correlations.

ACKNOWLEDGMENTS

The authors thank M. Akritidis for useful discussions. The simulations were performed at the Coventry university on the Zeus cluster with excellent technical support of A. Pedcenko.

Appendix A: I -Replica Cluster Algorithm

In this section we show that the I -replica cluster moves satisfy the detailed balance condition with respect to the I -replica Boltzmann distribution. Note that a similar derivation in case of the Ising ferromagnet can be found in [72]. The I -replica Hamiltonian for given a realization of bonds \mathbf{J} is given by

$$\mathcal{H}(\mathcal{S}) = H_{\mathbf{J}}^{(I)}(\mathcal{S}^{(1)}, \dots, \mathcal{S}^{(I)}) = - \sum_{\langle \mathbf{x}, \mathbf{y} \rangle} J_{\mathbf{x}\mathbf{y}} \tilde{s}_{\mathbf{x}} \tilde{s}_{\mathbf{y}}$$

$$\text{where } \tilde{s}_{\mathbf{x}} \tilde{s}_{\mathbf{y}} = \sum_{i=1}^I s_{\mathbf{x}}^{(i)} s_{\mathbf{y}}^{(i)}$$

and $\tilde{s}_{\mathbf{x}} = (s_{\mathbf{x}}^{(1)}, \dots, s_{\mathbf{x}}^{(I)})$. We denote a certain spin state $\mathcal{S}_{\mu} = (\mathcal{S}_{\mu}^{(1)}, \dots, \mathcal{S}_{\mu}^{(I)})$ with the index μ and its energy by $\mathcal{H}_{\mu} = \mathcal{H}(\mathcal{S}_{\mu})$. The cluster algorithm works as follows. First, each bond is occupied with probability $p_{\mathbf{x}\mathbf{y}}^{(\mu)}$, where $p_{\mathbf{x}\mathbf{y}}^{(\mu)} = 0$ if $J_{\mathbf{x}\mathbf{y}} \tilde{s}_{\mathbf{x}}^{(\mu)} \tilde{s}_{\mathbf{y}}^{(\mu)} \leq 0$. Occupied bonds connect spin sites that group together in clusters. The smallest clusters are isolated spins and each site belongs to a exactly one cluster. Of all clusters we randomly choose a fraction $f \in [0, 1]$ and we put all spin sites within these clusters into a single set called \mathcal{A} . Often the fraction is set to $f = 0.5$. The rest of the spins belong to the complement of \mathcal{A} , $\mathcal{A}^c = \mathcal{A} \setminus \mathcal{N}$, where \mathcal{N} is the set that contains all sites \mathbf{x} , such that $|\mathcal{N}| = N$. By this procedure we have created a partition which separates all sites into two sets. The cluster move is performed by flipping all I -component spins inside \mathcal{A} , i.e. $\tilde{s}_{\mathbf{x}}^{(\mu)} \rightarrow -\tilde{s}_{\mathbf{x}}^{(\mu)}, \forall \mathbf{x} \in \mathcal{A}$. Afterwards, the system is in spin state \mathcal{S}_{ν} .

We now we derive the occupation probabilities $p_{\mathbf{x}\mathbf{y}}$ that lead to transition probabilities between the states that satisfy the property of detailed balance. The condi-

tion of detailed balance is given by [73]

$$\frac{T(\mu \rightarrow \nu)}{T(\nu \rightarrow \mu)} = \frac{\mathcal{P}(\mathcal{S}_{\nu}|\mathbf{J})}{\mathcal{P}(\mathcal{S}_{\mu}|\mathbf{J})} = \exp \{-\beta (\mathcal{H}_{\nu} - \mathcal{H}_{\mu})\}. \quad (\text{A1})$$

Here, $T(\mu \rightarrow \nu)$ denotes the transition probability from spin state \mathcal{S}_{μ} to spin state \mathcal{S}_{ν} and $T(\nu \rightarrow \mu)$ is the probability of the inverted transition. The weight of the states within the I -replica Boltzmann distribution is given by $\mathcal{P}(\mathcal{S}_{\nu}|\mathbf{J})$ and $\mathcal{P}(\mathcal{S}_{\mu}|\mathbf{J})$, respectively. The right hand side of Eq. (A1) depends on the energies \mathcal{H}_{μ} and \mathcal{H}_{ν} . States μ and ν only differ from one another by the flipped spins inside of \mathcal{A} , i.e., $\tilde{s}_{\mathbf{x}}^{(\nu)} = \tilde{s}_{\mathbf{x}}^{(\mu)} \forall \mathbf{x} \in \mathcal{A}$ and $\tilde{s}_{\mathbf{x}}^{(\nu)} = -\tilde{s}_{\mathbf{x}}^{(\mu)} \forall \mathbf{x} \in \mathcal{A}^c$. Due to the global spin-flip symmetry of the Hamiltonian, $\mathcal{H}(\mathcal{S}) = \mathcal{H}(-\mathcal{S})$, neighboring spins within the identical set \mathcal{A} or \mathcal{A}^c contribute the same energy in both states. Thus, the energies of the states are

$$\begin{aligned} \mathcal{H}_{\mu} &= \mathcal{H}_{\mu}^{(\mathcal{A})} + \partial \mathcal{H}_{\mu} + \mathcal{H}_{\mu}^{(\mathcal{A}^c)}, \\ \mathcal{H}_{\nu} &= \mathcal{H}_{\nu}^{(\mathcal{A})} + \partial \mathcal{H}_{\nu} + \mathcal{H}_{\nu}^{(\mathcal{A}^c)} \\ &= \mathcal{H}_{\mu}^{(\mathcal{A})} + \partial \mathcal{H}_{\nu} + \mathcal{H}_{\mu}^{(\mathcal{A}^c)}. \end{aligned}$$

Here, $\mathcal{H}^{(\mathcal{A})}$ is the contribution to the energy of spins inside \mathcal{A} , $\mathcal{H}^{(\mathcal{A}^c)}$ is the contribution from spins which belong to \mathcal{A}^c and $\partial \mathcal{H}$ is the energy contribution of the surface of the partition. This surface is defined in terms of bonds which connect spins from \mathcal{A} with those of \mathcal{A}^c , i.e. $\partial \mathcal{A} = \{(\mathbf{x}, \mathbf{y}) \in \langle \mathbf{x}, \mathbf{y} \rangle : \mathbf{x} \in \mathcal{A} \wedge \mathbf{y} \in \mathcal{A}^c\}$. The energy difference of both states is proportional to the surface energy,

$$(\mathcal{H}_{\nu} - \mathcal{H}_{\mu}) = -2\partial \mathcal{H}_{\mu},$$

where we made use of the relation $\partial \mathcal{H}_{\nu} = -\partial \mathcal{H}_{\mu}$, which results from the fact that bonds in the surface which are broken in state μ are satisfied in state ν and vice versa. By broken and satisfied bonds we mean that $J_{\mathbf{x}\mathbf{y}} \tilde{s}_{\mathbf{x}} \tilde{s}_{\mathbf{y}} \leq 0$ and $J_{\mathbf{x}\mathbf{y}} \tilde{s}_{\mathbf{x}} \tilde{s}_{\mathbf{y}} > 0$, respectively. The energy of the surface can be written in terms of broken and satisfied bonds

$$\begin{aligned} \partial \mathcal{H}_{\mu} &= - \sum_{\partial \mathcal{A}_{\mu}^{+}} |J_{\mathbf{x}\mathbf{y}} \tilde{s}_{\mathbf{x}}^{(\mu)} \tilde{s}_{\mathbf{y}}^{(\mu)}| + \sum_{\partial \mathcal{A}_{\mu}^{-}} |J_{\mathbf{x}\mathbf{y}} \tilde{s}_{\mathbf{x}}^{(\mu)} \tilde{s}_{\mathbf{y}}^{(\mu)}| \\ &= - \sum_{\partial \mathcal{A}_{\mu}^{+}} J_{\mathbf{x}\mathbf{y}} \tilde{s}_{\mathbf{x}}^{(\mu)} \tilde{s}_{\mathbf{y}}^{(\mu)} + \sum_{\partial \mathcal{A}_{\mu}^{-}} J_{\mathbf{x}\mathbf{y}} \tilde{s}_{\mathbf{x}}^{(\nu)} \tilde{s}_{\mathbf{y}}^{(\nu)}. \end{aligned}$$

Here $\partial \mathcal{A}_{\mu}^{+}$ denotes the section in the surface where bonds are satisfied in state μ and $\partial \mathcal{A}_{\mu}^{-}$ the section with broken bonds. As already mentioned, $\partial \mathcal{A}_{\mu}^{+} = \partial \mathcal{A}_{\nu}^{-}$ and $\partial \mathcal{A}_{\mu}^{-} = \partial \mathcal{A}_{\nu}^{+}$.

Now the left hand side of equation (A1) is considered. The transition probability from state μ to ν can be written as

$$T(\mu \rightarrow \nu) = K(\mathcal{A} \wedge \mathcal{A}^c | \mu) \prod_{\partial \mathcal{A}_{\mu}^{+}} (1 - p_{\mathbf{x}\mathbf{y}}^{(\mu)}).$$

The first factor $K(\mathcal{A} \wedge \mathcal{A}^c | \mu)$ denotes the probability that the sets \mathcal{A} and \mathcal{A}^c are constructed given the state μ . The

second factor is the probability that satisfied bonds in the surface between \mathcal{A} and \mathcal{A}^c are not occupied. Bonds in the surface which are broken in state μ are not included because they are not occupied with probability one. The probability of the inverted transition from ν to μ is given by

$$T(\nu \rightarrow \mu) = K(\mathcal{A} \wedge \mathcal{A}^c | \nu) \prod_{\partial \mathcal{A}_\nu^+} (1 - p_{\mathbf{x}\mathbf{y}}^{(\nu)}).$$

Except for the bonds in the surface the identical bonds are broken or satisfied in both states μ and ν . As a consequence, the probability to construct the sets \mathcal{A} and \mathcal{A}^c starting from the state ν is equal to the probability to construct the same sets starting with μ , i.e. $K(\mathcal{A} \wedge \mathcal{A}^c | \nu) = K(\mathcal{A} \wedge \mathcal{A}^c | \mu)$. By inserting our results for the transition probabilities as well as the surface energy into Eq. (A1) one obtains,

$$\frac{K(\mathcal{A} \wedge \mathcal{A}^c | \mu) \prod_{\partial \mathcal{A}_\mu^+} (1 - p_{\mathbf{x}\mathbf{y}}^{(\mu)})}{K(\mathcal{A} \wedge \mathcal{A}^c | \mu) \prod_{\partial \mathcal{A}_\nu^+} (1 - p_{\mathbf{x}\mathbf{y}}^{(\nu)})} = \exp \left\{ -2\beta \left(\sum_{\partial \mathcal{A}_\mu^+} J_{\mathbf{x}\mathbf{y}} \tilde{s}_{\mathbf{x}}^{(\mu)} \tilde{s}_{\mathbf{y}}^{(\mu)} - \sum_{\partial \mathcal{A}_\nu^+} J_{\mathbf{x}\mathbf{y}} \tilde{s}_{\mathbf{x}}^{(\nu)} \tilde{s}_{\mathbf{y}}^{(\nu)} \right) \right\},$$

which can be rewritten as

$$\frac{\prod_{\partial \mathcal{A}_\mu^+} (1 - p_{\mathbf{x}\mathbf{y}}^{(\mu)})}{\exp \left\{ -2\beta \sum_{\partial \mathcal{A}_\mu^+} J_{\mathbf{x}\mathbf{y}} \tilde{s}_{\mathbf{x}}^{(\mu)} \tilde{s}_{\mathbf{y}}^{(\mu)} \right\}} = \frac{\prod_{\partial \mathcal{A}_\nu^+} (1 - p_{\mathbf{x}\mathbf{y}}^{(\nu)})}{\exp \left\{ -2\beta \sum_{\partial \mathcal{A}_\nu^+} J_{\mathbf{x}\mathbf{y}} \tilde{s}_{\mathbf{x}}^{(\nu)} \tilde{s}_{\mathbf{y}}^{(\nu)} \right\}}.$$

This equation is satisfied if

$$p_{\mathbf{x}\mathbf{y}} = 1 - \exp(-2\beta J_{\mathbf{x}\mathbf{y}} \tilde{s}_{\mathbf{x}} \tilde{s}_{\mathbf{y}})$$

and the condition of detailed balance is fulfilled. For $I = 2$ the algorithm is equivalent to the algorithm of Jörg [21] and the occupied bonds are equal to the blue bonds in the CMR representation [20].

-
- [1] C. Yamaguchi, *Progr. theo. phys.* **124**, 399 (2010).
 - [2] C. Yamaguchi, *Physica A: Statistical Mechanics and its Applications* **392**, 1263 (2013).
 - [3] D. Stauffer and A. Aharony, *Introduction to Percolation Theory* (Taylor & Francis, London, 1994).
 - [4] G. Grimmett, *The Random-Cluster Model* (Springer, Berlin, Heidelberg, 2004).
 - [5] M. Sahimi and A. G. Hunt, eds., *Complex Media and Percolation Theory* (Springer, New York, 2021).
 - [6] C. M. Fortuin and P. W. Kasteleyn, *Physica* **57**, 536 (1972).
 - [7] M. E. Fisher, *Physics* **3**, 255 (1967).
 - [8] A. Coniglio and W. Klein, *J. Phys. A* **13**, 2775 (1980).
 - [9] A. Coniglio and A. Fierro, “Correlated percolation,” in *Complex Media and Percolation Theory*, edited by M. Sahimi and A. G. Hunt (Springer, New York, 2021) pp. 61–81.
 - [10] R. H. Swendsen and J. S. Wang, *Phys. Rev. Lett.* **58**, 86 (1987).
 - [11] J. S. Wang and R. H. Swendsen, *Physica A* **167**, 565 (1990).
 - [12] K. Binder and A. P. Young, *Rev. Mod. Phys.* **58**, 801 (1986).
 - [13] D. L. Stein and C. M. Newman, *Spin Glasses and Complexity* (Princeton University Press, Princeton, 2013).
 - [14] M. Mézard, G. Parisi, and M. Virasoro, *Spin Glass Theory and Beyond* (World Scientific, Singapore, 1987).
 - [15] E. Bolthausen and A. Bovier, eds., *Spin Glasses* (Springer, Berlin, Heidelberg, 2007).
 - [16] L. De Arcangelis, A. Coniglio, and F. Peruggi, *EPL* **14**, 515 (1991).
 - [17] J. Houdayer, *The European Physical Journal B* **22**, 479 (2001).
 - [18] L. Chayes, J. Machta, and O. Redner, *J. stat. phys.* **93**, 17 (1998).
 - [19] O. Redner, J. Machta, and L. F. Chayes, *Phys. Rev. E* **58**, 2749 (1998).
 - [20] J. Machta, C. Newman, and D. Stein, *Journal of Statistical Physics* **130**, 113 (2008).
 - [21] T. Jörg, *Progress of Theoretical Physics Supplement* **157**, 349 (2005).
 - [22] C. M. Newman and D. L. Stein, in *Spin glasses*, edited by E. Bolthausen and A. Bovier (Springer, Berlin, Heidelberg, 2007) pp. 159–175.
 - [23] R. Kumar, J. Gross, W. Janke, and M. Weigel, *Eur. Phys. J. B* **93**, 1 (2020).
 - [24] M. Hasenbusch, A. Pelissetto, and E. Vicari, *Phys. Rev. B* **78**, 214205 (2008).
 - [25] A. P. Young and R. B. Stinchcombe, *J. Phys. C* **9**, 4419 (1976).
 - [26] A. Bray and M. Moore, in *Heidelberg Colloquium on Glassy Dynamics*, edited by J. van Hemmen and I. Morgenstern (Springer, Berlin, Heidelberg, 1987) pp. 121–153.
 - [27] A. K. Hartmann and A. P. Young, *Phys. Rev. B* **64**, 180404 (2001).
 - [28] J. Houdayer and A. K. Hartmann, *Physical Review B* **70**, 014418 (2004).
 - [29] H. G. Katzgraber, L. W. Lee, and A. P. Young, *Phys. Rev. B* **70**, 014417 (2004).
 - [30] L. Fernandez, E. Marinari, V. Martin-Mayor, G. Parisi, and J. Ruiz-Lorenzo, *Phys. Rev. B* **94**, 024402 (2016).

- [31] H. Khoshbakht and M. Weigel, Phys. Rev. B **97**, 064410 (2018).
- [32] H. G. Katzgraber, M. Palassini, and A. Young, Phys. Rev. B **63**, 184422 (2001).
- [33] P. Contucci, Journal of Physics A: Mathematical and General **36**, 10961 (2003).
- [34] P. Contucci and C. Giardina, Annales Henri Poincare **6**, 915 (2005).
- [35] P. Contucci and C. Giardina, Phys. Rev. B **72**, 014456 (2005).
- [36] P. Contucci, C. Giardina, C. Giberti, and C. Vernia, Phys. rev. lett. **96**, 217204 (2006).
- [37] C. M. Newman and D. L. Stein, in *Spin Glasses*, edited by E. Bolthausen and A. Bovier (Springer, Berlin, Heidelberg, 2007) pp. 145–158.
- [38] U. Wolff, Phys. Rev. Lett. **62**, 361 (1989).
- [39] R. H. Swendsen and J.-S. Wang, Phys. rev. lett. **57**, 2607 (1986).
- [40] U. Wolff, Phys. Lett. B **228**, 379 (1989).
- [41] M. E. Newman and G. T. Barkema, *Monte Carlo methods in statistical physics* (Oxford University Press, Oxford, 1999).
- [42] A. Coniglio, F. di Liberto, G. Monroy, and F. Peruggi, Phys. Rev. B **44**, 12605 (1991).
- [43] V. Cataudella, G. Franzese, M. Nicodemi, A. Scala, and A. Coniglio, Phys. Rev. Lett. **72**, 1541 (1994).
- [44] P. H. Lundow and I. Campbell, Phys. Rev. E **86**, 041121 (2012).
- [45] K. Binder and D. W. Heermann, “Theoretical foundations of the monte carlo method and its applications in statistical physics,” in *Monte Carlo Simulation in Statistical Physics: An Introduction* (Springer Berlin Heidelberg, Berlin, Heidelberg, 2010) pp. 5–67.
- [46] O. Melchert, “autoscale.py - a program for automatic finite-size scaling analyses: A user’s guide,” (2009), arXiv:0910.5403.
- [47] W. Janke and A. M. Schakel, Phys. Rev. E **71**, 036703 (2005).
- [48] M. Akritidis, N. G. Fytas, and M. Weigel, J. of Phys.: Conference Series **2207**, 012004 (2022).
- [49] H. Imaoka, H. Ikeda, and Y. Kasai, Physica A **246**, 18 (1997).
- [50] H. Fajen, A. K. Hartmann, and A. P. Young, Physical Review E **102**, 012131 (2020).
- [51] H. Nishimori, Progr. of Theo. Phys. **66**, 1169 (1981).
- [52] H. Nishimori, J. Phys. C **13**, 4071 (1980).
- [53] L. Bai and D. Breen, J. Graphics Tools **13**, 53 (2008).
- [54] Note that this implies that they are satisfied in *all* replicas for $I = 2$.
- [55] T. Jörg, Phys. Rev. B **73**, 224431 (2006).
- [56] Note that in the framework of the graphical representation of Chayes, Machta and Redner CMRJ clusters are denoted as “blue” clusters, see [20] for details.
- [57] A. P. Young, *Everything You Wanted to Know About Data Analysis and Fitting but Were Afraid to Ask* (Springer, Cham, 2015).
- [58] Y. R. Pei and M. Di Ventura, “A finite-temperature phase transition for the ising spin-glass in $d \geq 2$,” (2021).
- [59] Note that, using more replicas in Eq. (15) notably reduces the occupation probability and thus lowers the temperature of percolation. As a consequence, it might be interesting to see if for a certain I the percolation transition is directly linked to the spin glass transition if it occurs at non-zero temperatures.
- [60] H. G. Katzgraber, M. Körner, and A. Young, Phys. Rev. B **73**, 224432 (2006).
- [61] M. Baity-Jesi, R. Baños, A. Cruz, L. A. Fernandez, J. M. Gil-Narvion, A. Gordillo-Guerrero, D. Iniguez, A. Maiorano, F. Mantovani, E. Marinari, *et al.*, Phys. Rev. B **88**, 224416 (2013).
- [62] J. Machta, C. M. Newman, and D. L. Stein, in *Spin glasses: Statics and dynamics* (2009) pp. 205–223.
- [63] A. Coniglio, C. R. Nappi, F. Peruggi, and L. Russo, Comm. Math. Phys. **51**, 315 (1976).
- [64] Z. Zhu, A. J. Ochoa, and H. G. Katzgraber, Phys. Rev. Lett. **115**, 077201 (2015).
- [65] P. H. Lundow and I. Campbell, Phys. Rev. E **86**, 041121 (2012).
- [66] D. Kandel and E. Domany, Phys. Rev. B **43**, 8539 (1991).
- [67] V. Cataudella, G. Franzese, M. Nicodemi, A. Scala, and A. Coniglio, Phys. Rev. E **54**, 175 (1996).
- [68] J. Liu, Y. Qi, Z. Y. Meng, and L. Fu, Phys. Rev. B **95**, 041101 (2017).
- [69] B. McNaughton, M. V. Milošević, A. Perali, and S. Pilati, Phys. Rev. E **101**, 053312 (2020).
- [70] L. Wang, Phys. Rev. E **96**, 051301 (2017).
- [71] Y. R. Pei and M. Di Ventura, Phys. A **591**, 126727 (2022).
- [72] W. Krauth, in *New Optimization Algorithms in Physics*, edited by A. K. Hartmann and H. Rieger (Wiley-VCH, Weinheim, 2004) p. 7.
- [73] M. Newman and G. Barkema, *Monte carlo methods in statistical physics* (Oxford University Press, Oxford, 1999).